SUPERCRITICAL FLOW AROUND AND BENEATH A FIXED OBSTACLE

Nicolas Rivière[1], Anne-Gaëlle Laïly[1], Emmanuel Mignot[1], Delphine Doppler[1]

[1] Laboratory of Fluid Mechanics and Acoustics (LMFA)
CNRS / Université de Lyon (ECL, INSA, UCBL), 69621 Villeurbanne Cedex, France
E-mail: nicolas.riviere@insa-lyon.fr

Abstract

This paper presents an experimental study of the interaction between a supercritical, uniform turbulent, open channel flow and a fixed, emerged rectangular obstacle. The two main structures located upstream from the obstacle in such flows are a detached hydraulic jump and a horseshoe vortex. Their positions are assessed using photographs and oil flow visualizations. A laser grid projection technique is developed to provide water depth maps around the obstacle. This obstacle can be on contact with the channel bed or slightly above. It allows studying the influences on the flow of both the obstacle width and the gap below the obstacle. Compared to existing literature, present work assesses the existence of a new flow type – the so-called "coincident" type – where the toes of the hydraulic jump and of the horseshoe vortex are located at the same distance from the obstacle.

Introduction

This paper goes on preceding works aiming to characterize the interaction of a uniform supercritical open channel flow with an emerged obstacle.

The interaction of a subcritical open channel flow with an impervious emerging obstacle standing on a fixed bed has been deeply investigated in the literature. As the inflow approaches the obstacle, the adverse pressure gradient between the upstream flow and the flow at the upstream face of the obstacle leads to a boundary layer separation in the near-bottom region. This separation gives birth to a horseshoe vortex (HSV) on the upstream side of the obstacle (Dargahi (1989) or Sahin *et al.*, 2007). Authors such as Graf and Yulistiyanto (1998), Ahmed and Rajaratnam (1998), Sadeque *et al.* (2008) or Roulund *et al.* (2005) observe that upstream from the horseshoe vortex, the near-bed streamwise velocity is directed towards the obstacle, with a negative shear stress and that reverse streamwise velocities with positive shear stress are measured within the horseshoe vortex near the bed. The location where the bed shear stress reaches a zero magnitude corresponds to the separation point of the boundary layer and thus to the upstream limit of the horseshoe vortex.

Works related to the interaction between a supercritical open channel inflow and an obstacle are limited. Jiang and Smith (2000) report that a stationary shock wave takes place in front of the obstacle. The shape of the shock is a bow wave near the centerline and a V-wave further away. Near the centerline, the shock is perpendicular to the flow axis and past the jump the flow becomes subcritical and is deflected away from the centerline to pass on the sides of the obstacle. Further from the centerline, the supercritical inflow experiences an oblique jump at the trailing edge of the V-wave and the flow downstream from the jump remains supercritical with a deflected flow direction as predicted by Ippen (1951). Such flow pattern presents strong analogies with works performed on detached shock waves upstream bluff bodies which have been undertaken for decades, essentially for aerodynamic purposes (see Shapiro, 1953). More recently, Mignot and Rivière (2010) and Mignot *et al.* (2011) have investigated the interaction between a supercritical open channel inflow and a rectangular shaped obstacle focusing particularly on the detachment length of the hydraulic jump. These works reveal that depending on the Reynolds number of the inflow, two flow types can be observed, which are defined by the ratio labeled "Λ" (with $\Lambda=\lambda_J/\lambda_H$) between the detachment length of the hydraulic jump λ_J and that of the horseshoe vortex λ_H. For a turbulent inflow, the flow type is called "breaking": the detachment length of the hydraulic jump exceeds the detachment length of the horseshoe vortex ($\Lambda>1$). The flow first reaches a detached, bow-like, hydraulic jump, passes to a subcritical regime and then reaches the horseshoe vortex which acts as a positive step, leading to a sudden increase of the water depth (see Figure 1). Finally the flow passes around the obstacle. The aim of the present paper is to investigate the influence of a gap below the obstacle and the influence of upstream disturbances on the behavior of the two structures, hydraulic jump and horseshoe vortex in a breaking type flow.

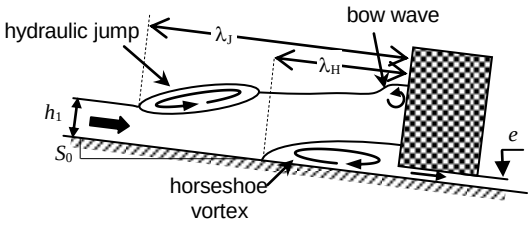

Figure 1: Side view in the symmetry plane of the flow

In a first step, we experimentally study the influence of the gap on the detachment lengths. In a second step, we investigate the effect of upstream flow disturbances that radically change the interaction between the horseshoe vortex and the jump.

Experiments

Experimental set-up

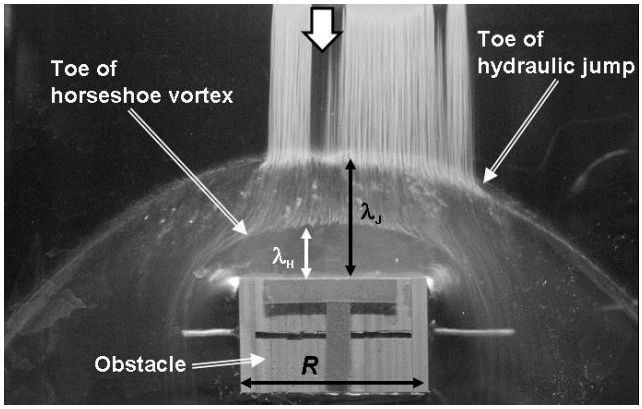

Figure 2: Visualization of hydraulic jump and horseshoe vortex around the obstacle, viewed from below (from Mignot and Rivière, 2010).

The experimental set up at LMFA in Lyon is described in Mignot and Rivière (2010). The experiments are performed in a smooth, transparent, L=118 cm long, and b=74.5 cm wide water table with adjustable slope S_0. The water passes through an upstream stilling basin, perforated plates, a grillage buffer and reaches the water table through a vertical, rounded step. In absence of lateral constriction, no shock-wave develop at the free surface and the flow rapidly reaches the uniform flow depth h_1 (see fig.1) defined by the combination of slope and discharge. Small residual surface waves, characteristic of supercritical flows, can be suppressed by modifying the surface tension with no effect on the results (Mignot and Rivière, 2010). h_1 is measured manually using a digital limnimeter (uncertainty of 0.2 mm). Discharge Q is measured by an electromagnetic flowmeter (uncertainty 0.01 L/s). The emerging obstacle is placed on the water table about 90 cm downstream from the stilling basin. The test section thus starts 50 cm downstream from the stilling basin, which is more than 100 times h_1. This is more than the ratio required to obtain a fully developed flow according to observations with comparable Reynolds numbers (Ranga Raju *et al.*, 2000; Kirkgoz and Ardiçhoglu, 1997). The obstacle is made of several 2 or 10 mm thick individual squared plastic plates maintained together, enabling a rapid and precise modification of the obstacle width R. A 14 mm opening camera is fixed to the water table support, under the water-table plane, just below the obstacle. The horseshoe vortex is visualized from the bottom by releasing gouache paint upstream from the obstacle (oil flow visualization); the toe of the hydraulic jump is visualized by the white, bright line corresponding to the abrupt change of the water depth or free-surface gradient (fig.2).

Laser grid technique for the water depth measurements

In order to measure the water depth around the obstacle, a laser grid technique has been developed. We project points which allow easier image processing than fringe patterns. A laser is fitted with special optical lenses that split the beam into 11x11 narrow beams tilted up to 28° relatively to the main laser axis. The laser is placed perpendicularly to the water table above the flow and allows to project a grid of N = 11 x 11 regularly spaced points on a 200 mm x 200 mm wide zone on the water flow which has been made opaque by diluting small amount of white dye in the stilling tank. A camera is positioned side-looking relatively to the water table, with its axis perpendicular to the streamwise axis but inclined in regard to the horizontal (Fig 3). The image obtained with no water flow *(h=0)* is called the *reference image* (labeled "0") and contains N points M_j^0 (j=1…N) with coordinates in the camera image frame (labeled "i") $(x_i(j,0), y_i(j,0))$. In presence of a water flow, the intersection P_j^h of each laser beam j with the water surface of local elevation $h(x,y)$ has coordinates (x,y,h) in the water table frame. Each luminous point P_j^h is viewed on the camera image as a 30 pixels wide spot of center M_j^h with coordinates $(x_i(j,h), y_i(j,h))$ in the image frame (sensor plane on Fig 3).

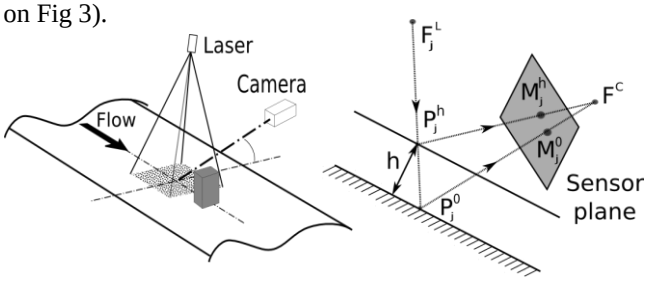

Figure 3: (left) Set-up (right) Illustration of the deviation of the image point for a water depth h, viewed in the plane containing the laser beam j of focal point F_j^L and the camera focal point F^C.

The principle of the method relies on two basic optical effects. Firstly, on the camera image any image point M_j^h exhibits a deviation $[x_i(j,h)-x_i(j,0)]$ (or $[y_i(j,h)-y_i(j,0)]$)

which is proportional to the local water depth $h(x,y)$ (fig. 3) with a coefficient α_j that depends on the laser beam j attached to the point P_j^h. Using this property, the N coefficients α_j are inferred from a calibration procedure performed by projecting the laser on calibration plates of controlled thickness. Secondly, due to the camera angle and the large depth in field used, length distortion has to be considered: for a regular laser grid, the further two points are from the camera focal point, the closer to each other they appear on the photo. This effect depends on the surface elevation. A second calibration procedure is thus needed (without laser) to establish the relationship between the (x,y) coordinates of the real intersection point of laser beam and free-surface and the image in-plane coordinates. We use a target (made of 19x27 points) drawn on four calibration plates, made of regularly spaced points of known actual coordinates (x,y,h). Image processing and linear interpolation are applied to determine a projection mapping $(x_i(h), y_i(h), h) \rightarrow (x,y,h)$. After calibration (determination of the α_j and of the projection mapping), for any image the measurement procedure is the following: *i)* the image coordinates (x_i, y_i) of the centers of the N image spots M_j^h are determined by image processing, *ii)* a laser beam j is attributed to each image point M_j^h, which is done by a semi-automated image processing including particle tracking between the image and the *reference image*, *iii)* the water depth is calculated using $h(x_i(j),y_i(j)) = [x_i(j)-x_i(j,0)] / \alpha_j$, *iv)* knowing h for each M_j^h, the real in-plane coordinates (x,y) of the water surface/laser intersections P_j^h are inferred from the projection mapping $(x_i(h), y_i(h), h) \rightarrow (x,y,h)$, *v)* the water depth map is deduced from linear interpolation of the actual coordinates (x,y,h) of the N measured points.

Dimensional analysis

The dimensional analysis, adapted from Mignot and Rivière (2010), defines the flow and obstacle parameters that affect the detachment length λ_J (resp. λ_H) of the hydraulic jump (resp. of the horseshoe vortex). Considering additionally that the Morton number characterizing the interface between water and air is constant, the dimensional analysis can be rewritten:

$$\frac{\lambda}{h_1} = f\left(Fr_1, \mathrm{Re}, \frac{R}{h_1}, \frac{e}{h_1}\right) \quad (1)$$

with $Fr_1=U_1/(gh_1)^{1/2}$ the inflow Froude number, $Re=4h_1U_1/\nu$ the inflow Reynolds number, U_1 the inflow mean velocity ($U_1=Q/bh_1$), h_1 the uniform inflow water depth, R the width of the obstacle and e the gap. Mignot and Rivière (2010) showed that – at least in the range of the present experiments – the Reynolds number has no influence on λ/h_1 when the incoming flow is turbulent.

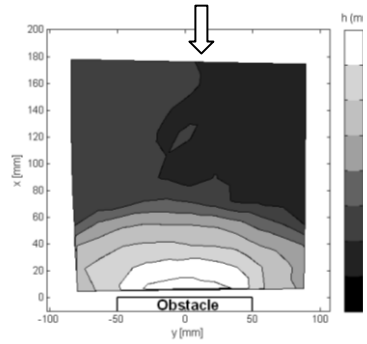

Figure 4: Water depth upstream from the obstacle (Breaking type; R=100 mm; e=0)

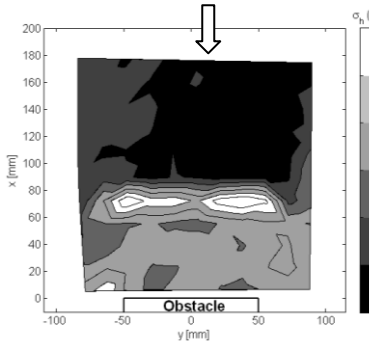

Figure 5: Standard deviation of water depth upstream from the obstacle (Breaking type; R=100 mm; e=0)

Their work also assessed the influence of the Froude number, which increase tends to decrease the detachment length λ_H of the horseshoe vortex, so as, but to a lesser extent, the detachment length λ_J of the hydraulic jump. As we focus here on the effect of the gap, in the experiments, the only varying parameters are e but also R by sake of comparison.

Experimental Results

Experimental conditions are: water depth h_1=5.15 mm, flow rate Q=2.05L/s, slope S_0=2.4%, so Re=11000 and Fr_1=2.38.

Mapping of the water depth and its variations

The water depth map (fig. 4) provides information on the behaviour of the whole free surface. It confirms the location of the toe of the jump measured from photographs (see Experimental set-up section) by Mignot and Rivière (2010).

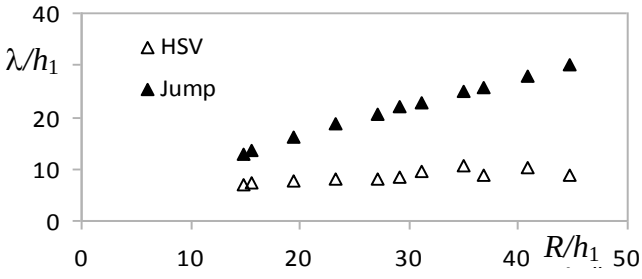

Figure 6: Influence of the obstacle length R on the detachment lengths (e=0)

It shows that the flow depth increases continuously from the toe of the jump to the stagnation point on the upstream face of the obstacle. The standard deviation map (fig.5) shows that strong free surface oscillations are located at the toe of the jump; they are far weaker near the stagnation point.

Influence of the obstacle length *R*

The influence of varying R with e=0 is sketched on figure 6. It confirms Mignot and Rivière (2010) results: increasing R causes an increase of the hydraulic jump detachment λ_J but has a weak influence on the horseshoe vortex HSV (λ_H). This can be explained by considering the mass conservation from the supercritical flow entering the jump to the critical flow outing from the subcritical zone between the shock and the body (fig.7). Such a mass conservation was derived first by Moeckel (1949) for compressible, supersonic flows around bluff bodies. Adapted by using equations for free-surface flows, it provides an analytical model predicting the location of the hydraulic jump (Mignot *et al.*, 2011). This model is accurate without horseshoe vortex (comparison with CFD results with slip condition on the bed) ; its predictions do not match with experiments as the vortex modifies both the location and shape of the effective critical section and the specific critical head, and thus affects the validity of the derivation involving L_c. Nevertheless, it is efficient in explaining how increasing R increases the discharge through the jump and thus causes an increase of L_c and thus of λ_J. As for the horseshoe vortex detachment length λ_H, it is driven by the balance between the adverse pressure gradient caused by the stagnation on the obstacle and the momentum of the incoming flow: this balance, so as λ_H, is not affected by the obstacle width (fig.6).

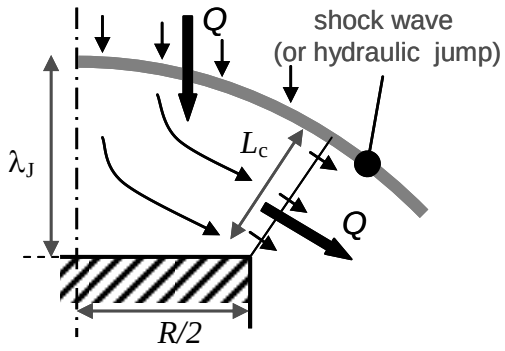

Figure 7: Flow through the jump and around the obstacle (top view)

Influence of the gap *e*

The influence of varying the gap e for R=76 mm is sketched on figure 8. Its increase shortens the jump

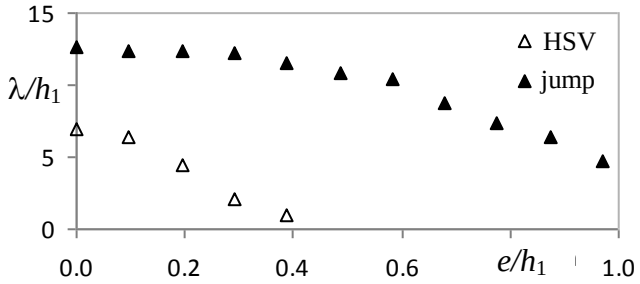

Figure 8: Influence of the gap e on the detachment lengths (R=76 mm)

detachment length λ_J. Indeed, part of the incoming discharge flows below the obstacle. For a given R, this shortens L_c and thus λ_J. Increasing e also shortens the horseshoe vortex detachment λ_H. Indeed, part of the flow reaccelerates to pass through the gap. It blows the boundary layer that reattaches below the obstacle; this was observed thanks to the oil (gouache) flow visualizations. When e and the flow discharge passing below the obstacle are high enough, the blowing of the boundary layer can even suppress the flow separation (e > 2mm *i.e.* e/h_1>0.4 on fig.8) and the horseshoe vortex. The influence of e and R being assessed in turbulent, supercritical, uniform flows, the work is now extended to a new flow configuration.

New flow type occurring in disturbed flows

In previous works (Mignot and Rivière, 2010), two flow patterns were identified. The first one, the so-called "separation type", occurs when the incoming supercritical flow is laminar; the toe of the horseshoe vortex is located upstream from the hydraulic jump (Λ<1). The second one, the so-called "breaking type" occurs when the incoming supercritical flow is turbulent; the toe of the hydraulic jump is then located upstream from the boundary layer separation (Λ>1). A third type can be obtained when an additional disturbance is applied to the incoming turbulent flow, upstream from the obstacle. Due to the respective locations of the toe of the horseshoe vortex and hydraulic jump (Λ=1, see next section), this kind of flow will be called "coincident type" in the sequel. In the present experiments, this disturbance was obtained thanks to Von Karmann streets produced by a point gauge (diameter 2 mm) stuck into the flow 40 cm upstream from the obstacle. Nevertheless, the same behavior was obtained when introducing other small bodies or when removing the stilling device (grillage buffer) at the water table inlet.

Flow features corresponding to the "coincident type"

The main characteristic of this flow type is indeed the coincident locations of the toe of the hydraulic jump and the horseshoe vortex *i.e.* $\lambda_J \approx \lambda_H$ or Λ=1. Oil (gouache) flow visualizations show that the horseshoe vortex is

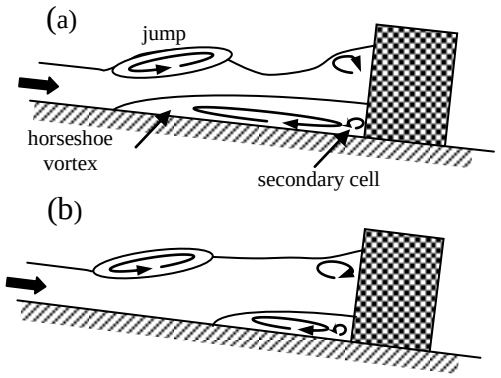

Figure 9: Flow features in coincident (a) and in breaking (b) types

always composed of one cell, plus the small secondary one at the obstacle/bed corner. Finally, the flow exhibits a characteristic shape of the free surface with a first raise corresponding to the hydraulic jump, a depression and then a second raise corresponding to the stagnation point (fig. 9-a). Indeed, the subcritical flow downstream the jump experiences an adverse slope caused by the presence of the horseshoe vortex; the water depth thus decreases before it increases again due to the influence of the stagnation point. In the "breaking type" (fig. 9-b), the flow is already influenced by the obstacle when it reaches the adverse slope; the water depth increases thus continuously downstream the jump.

Water depth field and its variations

Experimental conditions are the same as before (water depth h_1=5.15 mm, flow rate Q=2.05L/s, slope S_0=2.4%, resulting in Re=11007 and Fr_1=2.38). The water depth map (figure 10, which should be compared to figure 4) clearly shows the presence of two local maxima, the first one corresponding to the hydraulic jump, the second one to the stagnation point.

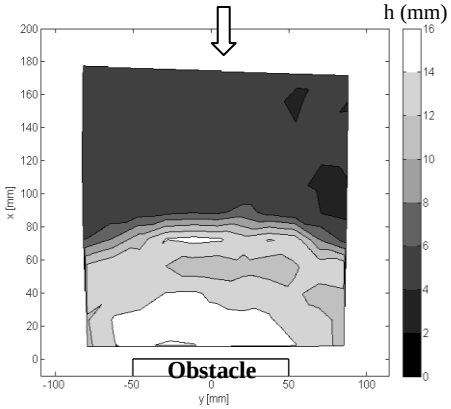

Figure 10: Water depths upstream from the obstacle (Coincident type; R=100 mm; e=0)

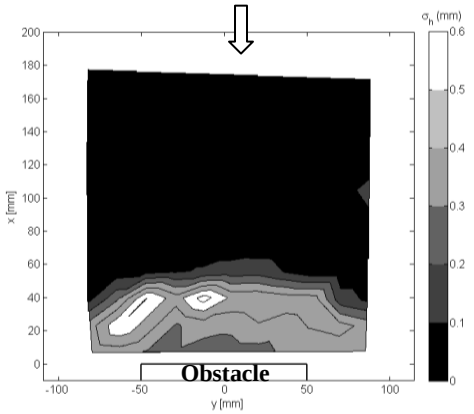

Figure 11: Standard deviation of water depths upstream from the obstacle (Coincident type; R=100 mm; e=0)

The standard deviation map (fig. 11) is more surprising. Indeed, the maximum standard deviation is located neither at the toe of the hydraulic jump, as it was for the breaking type (see fig. 5), nor at the stagnation point. It is located at the local minimum of the water depth.

Influence of the obstacle width *R*

This influence of R with e=0 for the coincident type flow is depicted on fig. 11. The two detachment lengths are equal (λ_H=λ_J) on the whole experimental range of R (circle symbols on fig. 12). When compared to breaking type, both lengths are closer to the one obtained for the hydraulic jump than to the one obtained for the horseshoe vortex. The influence of R, which increase increases the detachment lengths, was already explained thanks to the analogy with compressible flows.

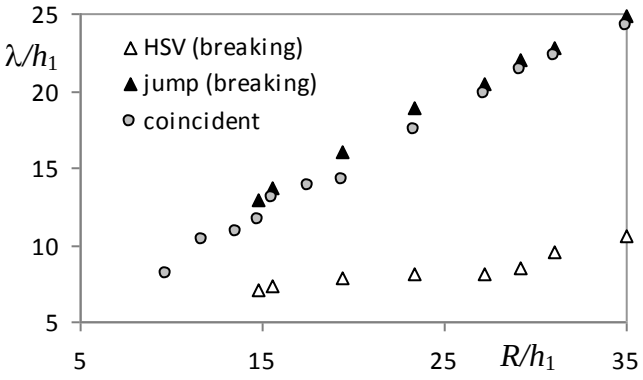

Figure 12: Effect of the obstacle width for the coincident mode (e=0)

Influence of the gap *e* below the obstacle

The influence of e for a coincident type flow (with R=76 mm) is comparable to the one observed in "breaking" type, explained thanks to the analogy with compressible flows. Coincident type flow behavior also confirms what was

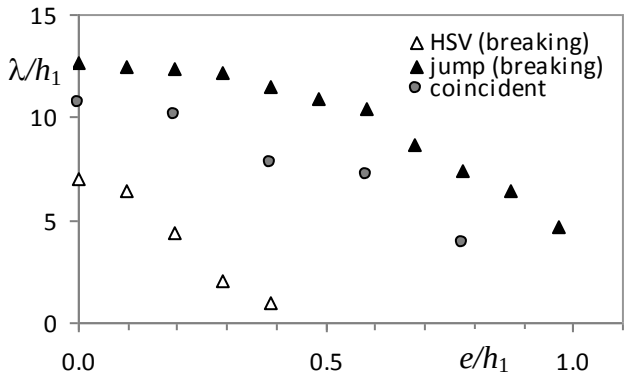

Figure 13: Effect of the gap e for the coincident mode (R=76mm)

obtained when varying R. First, the two detachment lengths are equal ($\lambda_H=\lambda_J$) on the whole experimental range of e. Second, the detachment length is intermediate between the ones obtained in breaking type for the jump and for the horseshoe vortex. This shows that the two structures (jump and vortex) interact and modify each other.

Discussion on the coincident mode

The change of behavior of the horseshoe vortex from the "breaking" mode to the "coincident" mode seems surprising. Indeed, the increase of turbulence usually tends to limit the flow separation and delay the horseshoe vortex appearance. In the present case, imposing additional disturbances tends to increase the size of the horseshoe vortex, that is anticipates the boundary layer separation. The cause is obviously the interaction with the hydraulic jump but, with the present measuring techniques, the detail of this interaction could not be investigated.

Conclusion

An experimental study of turbulent, supercritical flows around an obstacle, on contact with the channel bed or slightly above, was performed on a water table. The flow is characterized by a detached hydraulic jump and a horseshoe vortex located upstream from the obstacle. These two flow structures were characterized thanks to oil flow visualizations, while a laser grid technique was developed to measure the water depth around the obstacle.

These techniques were applied first on turbulent, supercritical, uniform flows. This is the so-called "breaking" type, as the hydraulic jump occurs upstream from the horseshoe vortex. Dimensional analysis shows that, apart from the Froude number, the two parameters that rule the flow are the dimensionless gap e/h_1 below the obstacle and the dimensionless obstacle width R/h_1. It was shown that these two parameters have opposite influences. Concerning the hydraulic jump, this was explained using the analogy with analytical modeling of detached shock waves. Concerning the horseshoe vortex, it can be reduced or even suppressed by the blowing of the boundary layer caused by the flow passing beneath the obstacle.

A second flow type was identified when introducing a disturbance upstream from the obstacle. It is the so-called "coincident" type, where the jump and the vortex occur at the same location, showing a strong interaction between the two structures. Taking benefit of this interaction, the control of the location of the horseshoe vortex, with applications for scouring, could be achieved by controlling the hydraulic jump location. Nevertheless, additional work should be devoted to check possible scale effects on the occurrence of both flow types. Notably, it is worth seeing if the increase of the Reynolds number up to field values can by itself promote the transition to the coincident mode without upstream disturbance, or can influence the flow pattern by enhancing air entrainment. Unfortunately, high Reynolds number flows would require the use of channels wider than the ones available in the laboratory at this time; future work will be devoted on these questions.

References

Ahmed, F., & Rajaratnam, N. (1998). Flow around bridge piers, *J. of Hydraul. Eng.* 124(3), pp. 288-300.

Chow, V. T. (1959). *Open channel hydraulics*, McGraw-Hill, New York.

Dargahi, B. (1989).The turbulent flow field around a circular cylinder, *Experiments in Fluids*, 8, pp. 1-12.

Graf, W.H. and Yulistiyanto, B. (1998). Experiments of flow around a cylinder; the velocity and vorticity fields, *J. of Eng. Mech.*, 36(4), pp. 637-653.

Ippen, A.T. (1951). Mechanics of supercritical flow: 1st paper of high velocity flow in open channels: A symposium, *Transactions ASCE*. 116, pp. 268-295.

Jiang, Q., & Smith, R.B. (2000). V-waves, bow shocks, and wakes in supercritical hydrostatic flows, *J. of Fluid Mech*. 406, pp. 27-53.

Kirkgoz and Ardiçhoglu (1997), Velocity profiles of developing and developed open channel flow, *J. Hydr. Eng.*, 123(12), pp. 1099-1105.

Mignot, E. and Rivière, N. (2010). Bow-wave like hydraulic jump and horseshoe vortex around an obstacle in a supercritical open channel flow, *Physics of Fluids*, 22, 117105.

Mignot, E., Rivière, N., & Chakraverty, K. (2011). Detached hydraulic jump upstream a fixed obstacle in supercritical flow. *34th IAHR Congress*, 26 June to 1st July 2011, Brisbane, Australia.

Moeckel, W.E. (1949). Approximate method for predicting form and location of detached shock waves ahead of planar or axially symmetric bodies, *National Advisory Committee for Aeronautics*, Technical note 1921, 32 pp.

Ranga Raju, K., Asawa, G., & Misra H. (2000). Flow establishment length in rectangular channels and ducts, *J. Hydraul. Eng*. 126, pp. 533-539

Roulund, A., Sumer, M., Fredsoe, J., & Michelsen, J. (2005). Numerical and experimental investigation of flow and scour around a circular pile, *J. Fluid Mech.*, 534, pp. 351-401.

Sadeque, M.A. Rajaratnam, N., & Loewen, M.R. (2008). Flow around cylinders in open channels, *J. of Eng. Mech.* 134(1), pp. 60-71.

Sahin, B. Ozturk, N.A., & Akilli, H. (2007), Horseshoe vortex system in the vicinity of the vertical cylinder mounted on a plate, *J. of Fluid Mech.* 18, pp.57-68.

Shapiro, A.H. (1953), *The dynamics and Thermodynamics of Compressible Fluid Flow*, Ronald Press, New-York, pp. 881-888.